

The Axisymmetric MRE Actuator in PIR control system

Abstract. This paper presents the results of a control system with a magnetorheological elastomers actuator. The device is configured axisymmetrical and it includes a permanent magnet. The idea of this work is to research the behaviour of intelligent material in the control system. The plant is controlled in a closed loop, where the feedback signal is the position of the membrane. We use proportional–integral–resonant controller and compare this algorithm with classical control algorithm – proportional–integral–derivative controller. This paper analyses the considered system by simulations and experiments. We present performance indexes of analyzed control algorithms in trajectory following a task.

Streszczenie. Ta publikacja prezentuje wyniki systemu sterowania silownika wykonanego z elastometru magnetoreologicznego. Urządzenie jest skonstruowane w sposób symetryczny i zawiera magnes trwałego. Celem pracy jest zbadanie zachowania inteligentnego materiału w systemie sterowania. Obiekt jest sterowany w zamkniętej pętli sprzężenia zwrotnego, w którym sygnałem zwrotnym jest pozycja membrany. Wykorzystany jest sterownik proporcjonalno-calkującąco-rezonansowy i jest porównywany z sterownikiem klasycznym – proporcjonalno-calkującąco-różniczkującym. W tej pracy analizowany jest system w symulacji i w eksperymentach. Wyniki porównawcze przedstawione są w postaci wskaźników całkowych dla zadania śledzenia trajektorii. (**Osiowo Symetryczny Silownik MRE z sterowaniem PIR**)

Keywords: magnetorheological elastomer actuator, smart material, PIR controller, PID controller

Słowa kluczowe: magnetoreologiczny silownik elastomerowy, materiał inteligentny, sterownik PIR, sterownik PID

Introduction

Smart actuators have had a great impact on research and practical applications in recent times. Smart materials such as magnetorheological elastomers, dielectric electroactive polymers or ionic polymer-metal composites can be applied to create advanced devices such as robotic grippers [1], interactive lens, speaker or pump [2]. In our work, we focus on the control problem of smart actuators. Control object is a round membrane made of magnetorheological elastomer (MRE) material with permanent magnet [3]. MRE materials are a combination of elastomer materials and magnetisable particles [4, 5]. One of the features of MRE is the ability to deform in the magnetic field like an artificial muscle. PIR controller [6] has a proportional and integral part similar to the PID controller. The last part R is called resonant and is tuned for the specific reference pulsation. This controller can be used for sinusoidal input signals with constant pulsation. It is worth pointing out that the PID controller was analyzed for a DEAP membrane [7, 8] that has a response similar to the presented device. The PIR controller has obtained great attention in recent time [9, 7, 10, 11]. The PID controller is a common regulation algorithm [12, 13]. This algorithm consists of three parts [13]: proportional–integral–derivative, where each of them is easy to interpret and analyse. These features make the PID controller convenient to tuning and simple to use.

The aim of this paper is to present the realisation of the control task implemented on a system with an actuator built on MRE material. The goal of the system is to control the actuator's position in the task trajectory following problem. The solution to this problem can be used in variable height and frequency speaker membrane or in micro pump could be controlled the liquid flow by frequency and chamber height. The problem is solved by simulations and experimental results. In our work, the main controller is PIR and the PID controller is used to compare results.

The Actuator Model

In this work, the MRE actuator is a plant in the control system. The concept of the actuator and its properties are presented in work [3]. In this work, we briefly introduce the main properties of the actuator to simplify the reading of a further part of the work. The actuator is built with an MRE membrane, permanent magnet, electromagnet and frame, as shown in Fig. 1. The input signal is a voltage to the electromagnet and the output is a displacement of the membrane

centre point. The identification of the actuator realized in the work [3] shown that the system can be described by Hammerstein model with the following transfer function:

$$(1) \quad v(t) = f_{nlr}(u(t)) \\ Y(s) = G_f(s)G_s(s)V(s)$$

where $u(t)$ is the input voltage, $v(t)$ is the internal signal (without physical meaning), $y(t)$ is the output displacement. The function $f_{nlr}(u) = c_3u^3 + c_2u^2 + c_1u$ is a polynomial which describes the input nonlinearity, the transfer function $G_f(s)$ defines fast dynamics and $G_s(s)$ is responsible for slow dynamics. Their exact definition is as follows:

$$(2) \quad G_s(s) = \frac{s + z_0}{s + s_0} \\ G_f(s) = \frac{k(\alpha^2 + \omega^2)}{s^2 + 2\alpha s + \alpha^2 + \omega^2}$$

where the parameters s_0 , z_0 define the zero and pole of the slow part and k , ω and α are the gain, damped natural frequency and decay ratio respectively. In our work, the analysis is performed based on the linearized plant model defined by:

$$(3) \quad G_p(s) = k_{nlr}G_s(s)G_f(s)$$

where k_{nlr} is gain of linear approximation of polynomial f_{nlr} .

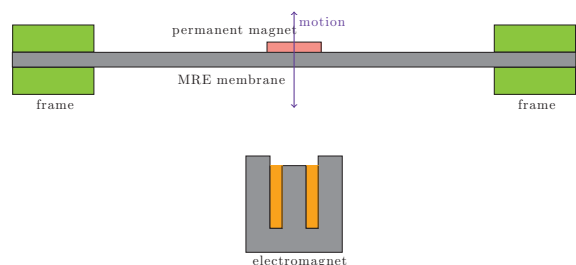


Fig. 1: The schema of axisymmetric MRE actuator with permanent magnet.

PIR and PID Controller

This section describes the ideas behind the control algorithms. The general concept of the control system has been shown in Fig. 2. In this figure, the trajectory generator block produces a reference signal mark as y_r . The next block is the

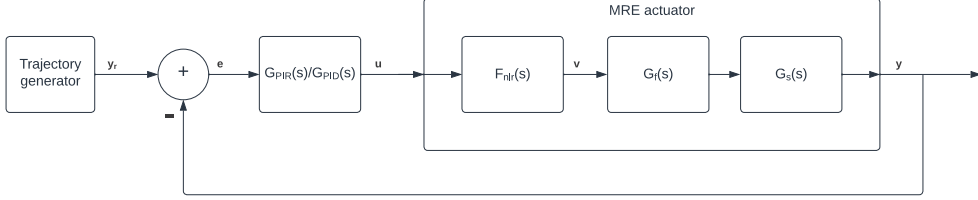


Fig. 2: Automatic control system diagram.

adder that operates to calculate the error $e = y_r - y$. The other signals are u , which is the control signal, and y is the output or measured signal. An important block is the position regulator, which implements PIR or PID controller. In summary, the plant is controlled in the closed control loop with two types of controllers: PIR and PID.

Both controllers have identical parts P and I, which can be described:

$$(4) \quad G_{PI}(s) = k_p + k_i \frac{1}{s}$$

The PIR controller will be described first. This controller is designed to track sinusoidal reference signals. In literature, many variants of this controller are presented, e.g. in [14] or in [15]. We have chosen a definition of PIR controller described in [7], which is given by:

$$(5) \quad G_{PIR}(s) = k_p + k_i \frac{1}{s} + k_r \frac{s}{s^2 + \omega_r^2}$$

where ω_r is pulsation reference signal, and parameters k_p , k_i , k_r are gains. The gain k_r creates the closed loop system with unit gain for the pulsation ω_r as it is visible in the following equations:

$$(6) \quad G_o(s) = (G_{PI}(s) + \frac{k_r s}{s^2 + \omega_r^2}) G_p(s)$$

$$(7) \quad G_z(s) = \frac{G_o(s)}{1 + G_o(s)}$$

$$(8) \quad G_z(s) = \frac{(G_{PI}(s) + \frac{k_r s}{s^2 + \omega_r^2}) G_p(s)}{1 + (G_{PI}(s) + \frac{k_r s}{s^2 + \omega_r^2}) G_p(s)}$$

$$(9) \quad G_z(s) = \frac{[G_{PI}(s)(s^2 + \omega_r^2) + k_r s] G_p(s)}{s^2 + \omega_r^2 + [G_{PI}(s)(s^2 + \omega_r^2) + k_r s] G_p(s)}$$

where $G_o(s)$ and $G_z(s)$ are transfer functions of open and closed loop systems respectively. Taking into account a fixed frequency $s = j\omega_r$, the transfer function of the closed loop system is given by:

$$(10) \quad G_z(j\omega_r) = \frac{k_r j\omega_r G_p(j\omega_r)}{k_r j\omega_r G_p(j\omega_r)} = 1$$

thanks to:

$$(11) \quad s^2 + \omega_r^2 = 0, \quad s = j\omega_r.$$

The $G_p(s)$ is a full transfer function plant. Second, is the PID controller, in which the equation is written as a transfer function as follows:

$$(12) \quad G_{PID}(s) = k_p + k_i \frac{1}{s} + k_d \frac{s}{sT_f + 1}$$

where T_f is filter time constant, k_p , k_i and k_d are gains of the controller. PID controller is well known and can be found in [12] or in [13]. This controller is used as a referential controller. Controllers were implemented as defined in (12) and (5) in a real device, so we change the domain from Laplace transform to a discrete form by using bilinear Z transformation $s = \frac{2(z-1)}{T_p(z+1)}$, where T_p is the sampling time.

Simulation Analysis

In this section, the simulation analysis of PIR and PID controllers for the MRE actuator is performed to obtain knowledge about the system behaviour under varying controller gains. The control system analysis is carried out based on the MRE actuator model defined in (1) and (2). To allow linear analysis, the polynomial is replaced by the linear gain calculated by linearization at the point $y = 0$. The parameters of the model are from work [3] and their values are as follows:

$$(13) \quad \begin{aligned} k &= 0.76 & \alpha &= 39.98 \\ \omega &= 246.11 & s_0 &= 0.13 \\ z_0 &= 0.17 & c_1 &= -8.24 \times 10^{-2} \\ c_3 &= 1.45 \times 10^{-5} & c_2 &= -1.66 \times 10^{-3} \end{aligned}$$

Initial controllers gains are set by trial and error method with a low k_p and k_i relying on the works [7, 8], where the gain of an integral part is much higher than a proportional part. It is worth pointing that our object has strong oscillations which are difficult to damp as described in the work [8]. Firstly, the PIR controller is analyzed with our actuator. This controller can decrease the following error for fixed frequency if the resonance part is enabled. Example of Bode plots for $\omega_r = 2\pi \cdot 10\text{Hz}$ and varying k_r are visible in Fig. 3. It is clear that for any positive gain k_r the closed loop gain is equal to 1 for pulsation ω_r thanks to $y = y_r$. Furthermore, the gain k_r is responsible for the width of the bandwidth. Secondly, we

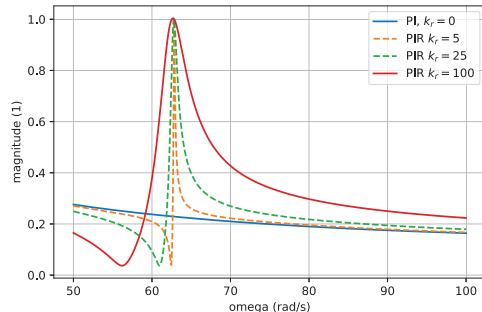


Fig. 3: The frequency characteristics of the closed loop system with PI and PIR controllers with $k_p = 1$ and $k_i = 400$.

focus on the analysis of the PID controller defined by (12). Similarly to the PIR controller, we simulated PID controller, the results of which are presented in Fig. 4. The closed loop gain decreases with the pulsation increase. To reduce this

feature, the k_i should be large. We test the k_d parameter on control impact, but a low value destabilizes the system, and we do not show these results.

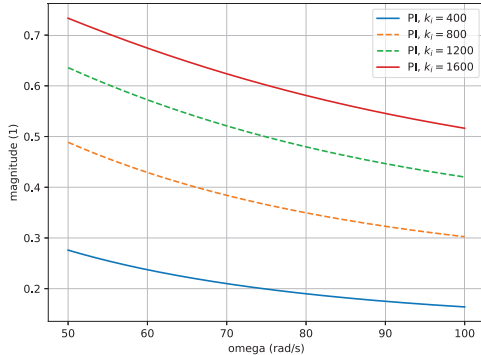


Fig. 4: The frequency characteristics of the closed loop system with PI controller with $k_p = 1$ and varying k_i .

Finally, the stability of the system with both controllers was checked by the Nyquist criterion. The stability of the closed system was analyzed based on the characteristics of the open loop $G_{ctr}(s) \cdot G_p(s)$ where $G_{ctr}(s)$ is the controller transfer function - for the PIR controller (5) and for the PID controller (12). The open loop for both controllers are stable because poles of each part of the system are on the left side of the plane of complex variable s. The results of the analysis are shown in Figs. 5 and 6.

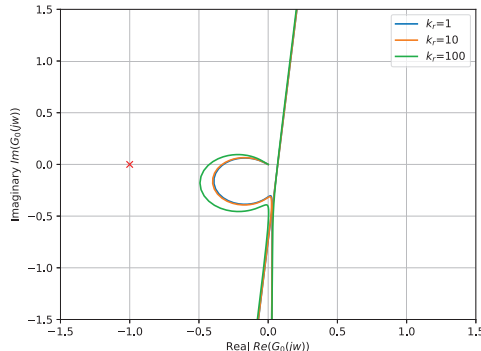


Fig. 5: The PIR controller stability analysis based on the Nyquist plot for various k_r gains.

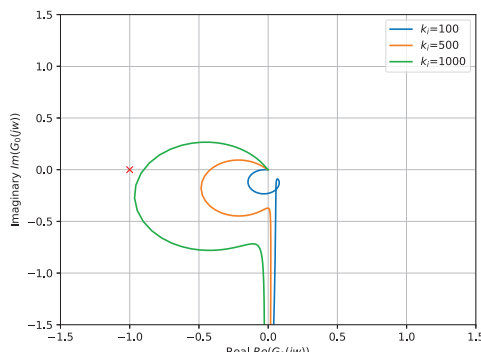


Fig. 6: The PID controller stability analysis based on the Nyquist plot for various k_i gains.

Experiments

In this section, we describe experimental results made after analysis simulations. The first step in the preparation of the experiment was to design and build the laboratory sta-

tion present in Fig. 7, which is based on aluminium profiles. The information about position provides laser sensor Micro-Epsilon optoNCDT 1900-25, which the main feature is high measure rate. The control laws are implemented in microcontroller Nucleo STM32F103RBTx with 72 MHz clock. The control signal u is applied to the electromagnet as a PWM signal driven by the H bridge (based on the component L6206). The range of u signal is from -12 V to 12 V . The data from the experiment are sent to a computer and saved on a hard disk.

In the experiments, the problem of following the reference trajectory was analysed. In this case, the sinusoidal reference is taken into account and the signal is defined as:

$$(14) \quad y_r(t) = A \sin(\omega_s t).$$

The parameter values for the signals are equal: $A = 0.5\text{ mm}$, $f = \{10, 30, 40\}(\text{Hz})$ ($\omega_s = 2\pi f$). To compare the quality of control for different controller parameters Integral Absolute Error (IAE) and Integral Time Absolute Error (ITAE) are defined as:

$$(15) \quad J_{IAE} = \int_0^{t_{end}} |e(t)| dt$$

$$J_{ITAE} = \int_0^{t_{end}} t |e(t)| dt,$$

where $e(t) = y_r(t) - y(t)$ is control error.

The PIR controller was used in the trajectory following the experiment. We tested different k_r values and different reference signal frequencies. The results of this experiment are presented in Table 1 for $f = 10\text{ Hz}$. For the PID controller, we set constant parameters values $k_p = 1.0$ and $k_d = 0.0$. The parameter k_i was varying. The results are summarised in Table 2. Looking for the first row of both tables values are similar, so the control quality is similar at the beginning of the experiment for both controllers. Analyzing the results from the table for PIR, increasing the value of k_r improves control quality. For $k_r = 100$, the values of J_{IAE} decrease about 95%. The impact of k_r parameter is presented in Fig. 8. In this figure, is presented how increase k_r parameter stabilises object control. It is worth to point that too large f (above 30 Hz) destabilises the system.

Table 1: Experiments result for PIR controller

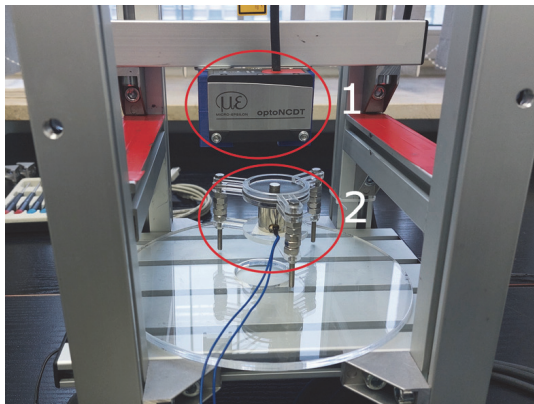
	$f = 10\text{Hz}, k_i = 400$	
k_r	J_{IAE}	J_{ITAE}
0	4 998.40	37 498.32
1	4 260.39	30 163.30
10	1 429.01	5 991.72
50	390.17	1 317.71
100	258.07	1 101.29

Analyzing values from Table 2 we see that the indicator values decrease by about 29% for $k_i = 2000$. The results are similar for J_{ITAE} . The impact of k_i parameter is also visible in Fig. 9 where for too small k_i the controller is too weak to follow the reference signal. For $k_i = 1400$ is visible phase shift and for too large k_i the system has a delay in reaction on the reference signal change.

The PIR controller reduces error better than the PID controller, about that say the lower J_{IAE} and J_{ITAE} values. The PIR controller have positive results in puls with constant frequency. Analysing the control signal u for both control al-

gorithms (Fig. 9, 8) we see that the signal does not enter saturation, so the wind-up does not occur.

a)



b)

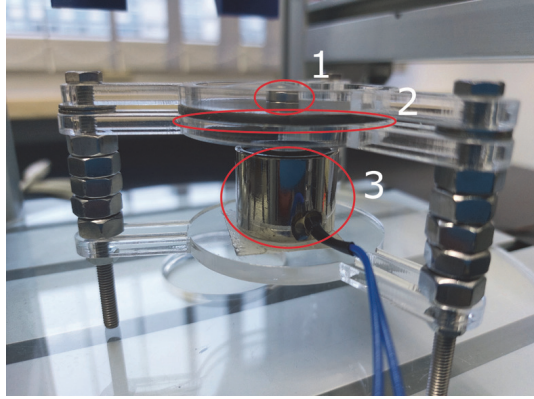
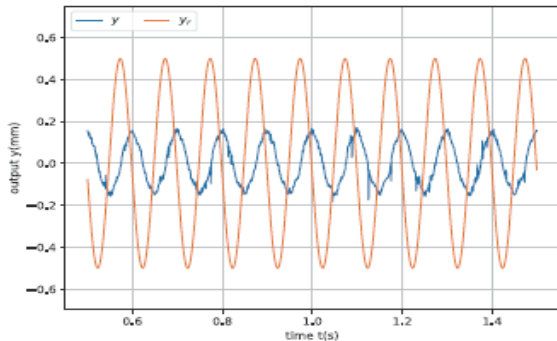


Fig. 7: The overall view on laboratory station (a): 1 - laser sensor, 2 - control object and close up view of the control object(b); 1 - permanent magnet, 2 - MRE membrane, 3 - electromagnet.

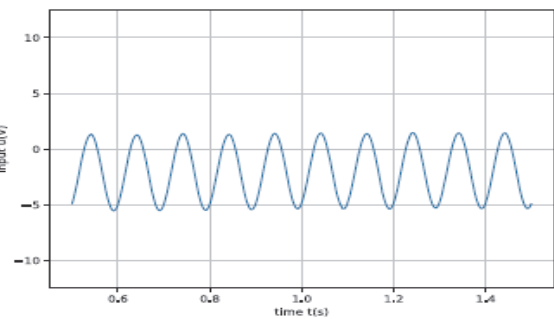
Table 2: Experiments result for PID controller

$f = 10\text{Hz}$			
k_i	J_{IAE}	J_{ITAE}	
100	4 721.56	35 389.90	
300	4 913.06	36 838.75	
500	5 066.14	38 014.60	
600	5 111.59	38 279.77	
800	5 111.27	38 326.46	
1000	4 974.03	37 290.73	
1200	4 702.46	35 248.85	
1400	4 360.53	32 705.48	
1600	4 005.27	30 052.38	
1800	3 669.06	27 488.24	
2000	3 357.83	25 156.49	

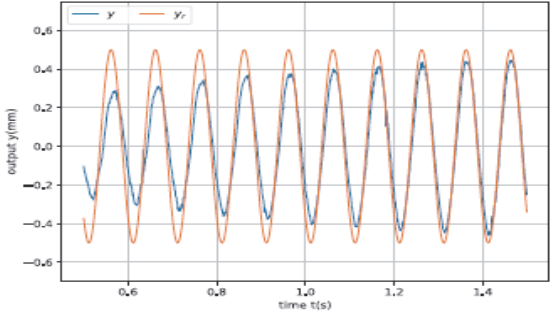
a)



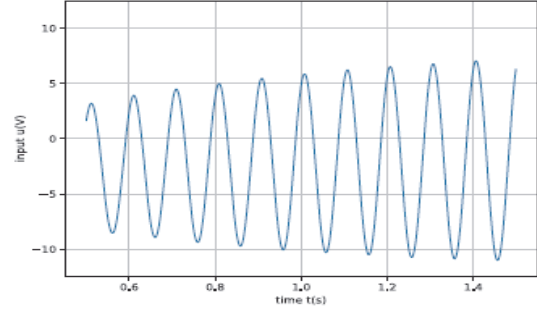
b)



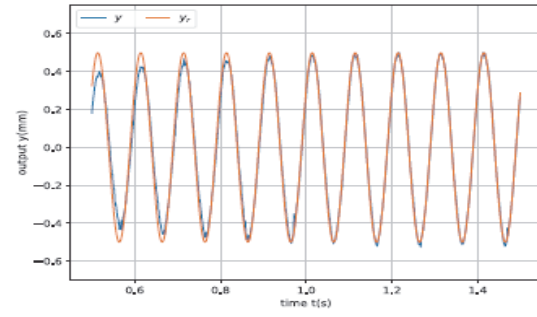
c)



d)



e)



f)

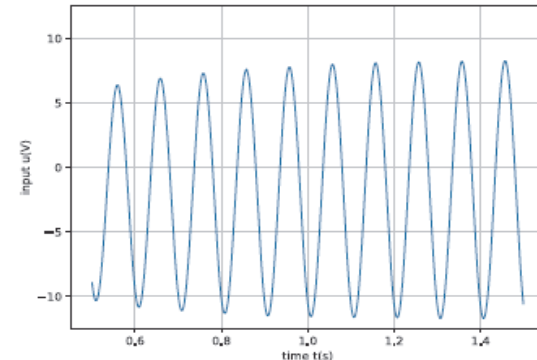
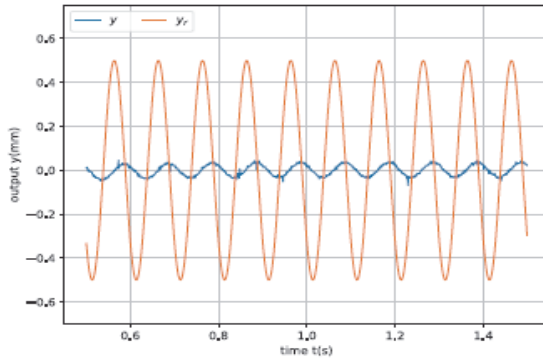
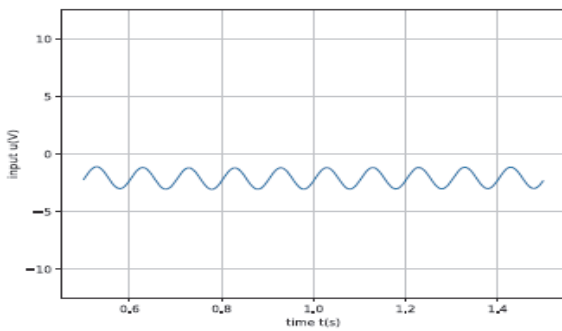


Fig. 8: The trajectory following problem for different kr values PIR controller. On the left side are compare signals yr and y , and on the right is u signal. For all figures, $kp = 1.0$, $ki = 400$ and $f = 10$. Figs. a), b) is for $kr = 0$; c), d) is for $kr = 50$; and e), f) is for $kr = 100$.

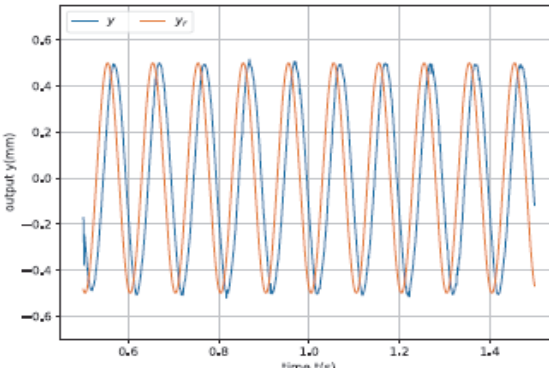
a)



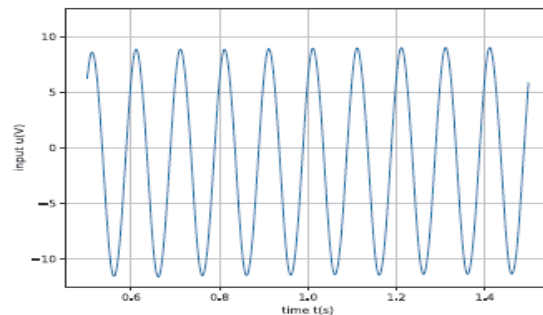
b)



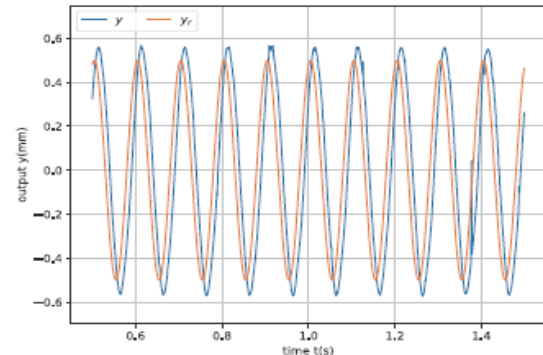
c)



d)



e)



f)

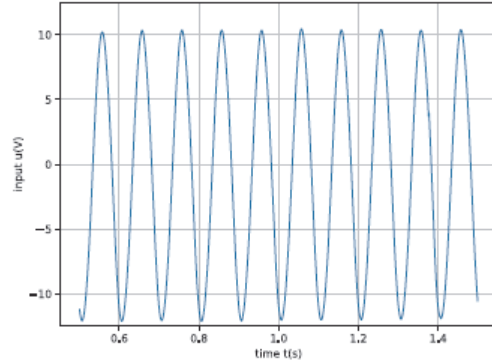


Fig. 9: The trajectory control for different ki values in PID controller. On the left side are compare signals y_r and y , and on the right is u signal. Figs. a), b) is for $ki = 100$, $kd = 0$; c), d) is for $ki = 1400$, $kd = 0$; and e), f) is for $ki = 2000$, $kd = 0$.

Conclusions

This paper investigates classical controllers for the purpose of controlling modern smart materials. We control the nonlinear MRE actuator with a permanent magnet by using PIR and PID controllers. The algorithms work out in our control task, which proves about these controllers are robust to object nonlinearity. Correctly setting controllers parameters values allows for reducing control error for small signal frequencies. The simulation and experimental analysis showed the same results. The PIR controller is better than the PID controller. The advantage of the PIR controller is that a model of the plant is not needed. However, the disadvantage of PIR is that this controller can be used only for a sinusoidal signal type and constant frequency.

Acknowledge

This research was funded by the Ministry of Education and Science, grant number 0211/SBAD/0122.

Authors: M. Sc. Paweł Czopek, Ph. D. Jakub Bernat, Institute of Automatic Control and Robotics, Faculty of Control, Robotics & Electrical Engineering, Poznań University of Technology, ul. Piastrowo 3A, 60-965 Poznań, Poland, email: pawel.czopek@put.poznan.pl

REFERENCES

- 1 N. Bira, P. Dhagat, and J. R. Davidson, "A review of magnetic elastomers and their role in soft robotics," *Frontiers in Robotics and AI*, vol. 7, 2020.
- 2 S.-Y. Tang, X. Zhang, S. Sun, D. Yuan, Q. Zhao, S. Yan, L. Deng, G. Yun, J. Zhang, S. Zhang, and W. Li, "Versatile microfluidic platforms enabled by novel magnetorheological elastomer microactuators," *Advanced Functional Materials*, vol. 28, p. 1705484, 2018
- 3 J. Bernat, P. Superczynska, P. Gajewski, A. Marcinkowska, "Magnetorheological axisymmetric actuator with permanent magnet," 2022. [Online]. Available: <https://arxiv.org/abs/2210.15968>
- 4 T. Liu and Y. Xu, "Magnetorheological elastomers: Materials and applications," in *Smart and Functional Soft Materials*, X. Dong, Ed. Rijeka: IntechOpen, 2019, ch. 4.
- 5 H. Böse, T. Gerlach, and J. Ehrlich, "Magnetorheological elastomers — an underestimated class of soft actuator materials," *Journal of Intelligent Material Systems and Structures*, vol. 32, no. 14, pp. 1550–1564, 2021.
- 6 V. D. Yurkevich, "Pir-controller design based on time-scale separation method and internal model principle for harmonics disturbances suppression," *Optoelectronics, Instrumentation and Data Processing*, vol. 57, no. 4, pp. 363–370, 2021, cited By :2. [Online]. Available: www.scopus.com
- 7 G. Rizzello, D. Naso, A. York, and S. Seelecke, "Modeling, identification, and control of a dielectric electro-active polymer

- positioning system," *IEEE Transactions on Control Systems Technology*, vol. 23, no. 2, pp. 632–643, 2015
- 8 J. Bernat and J. Kolota, "A pi controller with a robust adaptive law for a dielectric electroactive polymer actuator," *Electronics*, vol. 10, no. 11, 2021.
 - 9 D. Zmood and D. Holmes, "Stationary frame current regulation of pwm inverters with zero steady-state error," *IEEE Transactions on Power Electronics*, vol. 18, no. 3, pp. 814–822, 2003.
 - 10 J. Chen, W. Zhang, B. Chen, and Y. Ma, "Improved vector control of brushless doubly fed induction generator under unbalanced grid conditions for offshore wind power generation," *IEEE Transactions on Energy Conversion*, vol. 31, no. 1, pp. 293–302, 2016.
 - 11 C. Xia, B. Ji, and Y. Yan, "Smooth speed control for low-speed high-torque permanent-magnet synchronous motor using proportional– integral–resonant controller," *IEEE Transactions on Industrial Electronics*, vol. 62, no. 4, pp. 2123–2134, 2015.
 - 12 K. H. Ang, G. Chong, and Y. Li, "Pid control system analysis, design, and technology," *IEEE Transactions on Control Systems Technology*, vol. 13, no. 4, pp. 559–576, 2005.
 - 13 K. J. Astrom and R. M. Murray, *Feedback Systems: An Introduction for Scientists and Engineers*. USA: Princeton University Press, 2008.
 - 14 C. Xia, B. Ji, and Y. Yan, "Smooth speed control for low-speed high-torque permanent-magnet synchronous motor using proportional– integral–resonant controller," *IEEE Transactions on Industrial Electronics*, vol. 62, no. 4, pp. 2123–2134, 2015.
 - 15 M. Liserre, R. Teodorescu, and F. Blaabjerg, "Multiple harmonics control for three-phase grid converter systems with the use of pi-res current controller in a rotating frame," *IEEE Transactions on Power Electronics*, vol. 21, no